Computers and Mathematics with Applications 61 (2011) 1167–1179

Contents lists available at ScienceDirect

Computers and Mathematics with Applications

journal homepage: www.elsevier.com/locate/camwa

Numerical study of unsteady hydromagnetic Generalized Couette flow of a reactive third-grade fluid with asymmetric convective cooling

O.D. Makinde [a,*], T. Chinyoka [b]

[a] Institute for Advance Research in Mathematical Modeling and Computations, Cape Peninsula University of Technology, P.O. Box 1906, Bellville 7535, South Africa
[b] Center for Research in Computational and Applied Mechanics, University of Cape Town, Rondebosch 7701, South Africa

ARTICLE INFO

Article history:
Received 23 April 2010
Received in revised form 26 December 2010
Accepted 27 December 2010

Keywords:
Unsteady flow
Third grade fluid
Magnetohydrodynamics
Variable viscosity
Chemical kinetics
Finite difference method

ABSTRACT

Unsteady hydromagnetic Generalized Couette flow and heat transfer characteristics of a reactive variable viscosity incompressible electrically conducting third grade fluid in a channel with asymmetric convective cooling at the walls in the presence of uniform transverse magnetic field is studied. It is assumed that the chemical kinetics in the flow system is exothermic and the convective heat transfer at the channel surface with the surrounding environment follow the Newton's law of cooling. The coupled nonlinear partial differential equations governing the problem are derived and solved numerically using an unconditionally stable and convergent semi-implicit finite difference scheme. Both numerical and graphical results are presented and physical aspects of the problem are discussed with respect to various parameters embedded in the system.

1. Introduction

Hydromagnetic fluid flow continues to attract the attention of researchers due to its considerable practical application in nuclear engineering control, plasma aerodynamics, mechanical engineering manufacturing processes, astrophysical fluid dynamics, and Magnetohydrodynamic (MHD) energy systems [1–3]. The pioneering work of Hartmann [4] is regarded as the origin of MHD channel flow. He studied flow of a viscous incompressible electrically conducting fluid within a parallel plate channel in the presence of a transverse magnetic field. The main features of this flow are that the magnetic field produces viscosity and thereby offers rigidity to the fluid and, for large values of the Hartmann number, the flow within the channel is divided into two regions, namely the boundary layer region and central core region [5–7]. The boundary layer region is confined to a thin boundary layer which arises near the walls of the channel. This boundary layer is known as the Hartmann boundary layer. The change in the velocity and induced magnetic field is very rapid in this region. In the central core region, i.e. outside the boundary layer region, the velocity and induced magnetic field are almost uniform.

Of particular note is the fact that the flow behavior of most fluids used in industrial and engineering processes cannot be adequately explained on the basis of the classical, Newtonian viscous model. Examples include hot rolling, drilling muds, hydrocarbon oils, polyglycols, synthetic esters, polyphenylethers, oil and greases, clay coating and suspensions, paper products and many others. Several constitutive models have been suggested to characterize such non-Newtonian flow behavior. Among the many proposed models is the class of third order fluids for which one can reasonably hope to obtain a numerical solution. Extensive studies have been undertaken which involve such fluids [8–10]. Rajagopal [11] studied in detail the general thermodynamics, stability and uniqueness of fluids of the differential type with the fluid of third grade being a special case. For problems involving heat transfer for fluids of third grade, a complete thermodynamics analysis

* Corresponding author. Tel.: +27 21 9596641; fax: +27 21 5550775.
E-mail addresses: makinded@cput.ac.za (O.D. Makinde), tchinyok@vt.edu (T. Chinyoka).

0898-1221/$ – see front matter © 2010 Elsevier Ltd. All rights reserved.
doi:10.1016/j.camwa.2010.12.066

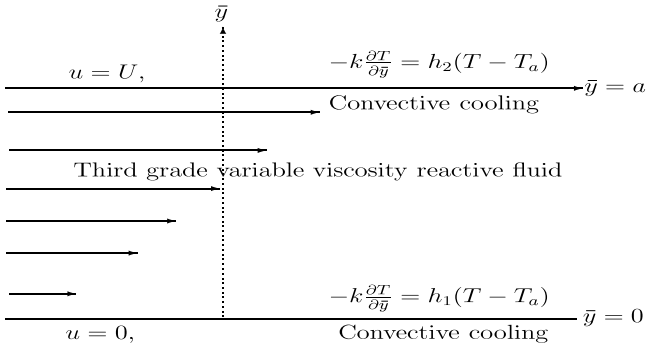

Fig. 1. Geometry of the problem.

of the constitutive function has been performed by Fosdick and Rajagopal [12]. Several studies involving heat and mass transfer in non-Newtonian third grade fluids have been conducted [13–15]. In the past, much attention was given to the time-independent channel flows of non-Newtonian fluid induced by the combined action of axial pressure gradient and uniform velocity of one of the walls in the presence of magnetic field [16]. Little attention has been devoted to examining time-dependent flow of non-Newtonian fluid problems. In recent times, Sajid et al. [17] considered the unsteady flow and heat transfer of a second grade fluid over a stretching sheet.

The objective of the present paper is to study unsteady hydromagnetic flow of a reactive variable viscosity incompressible electrically conducting third grade fluid between a moving and a fixed wall in the presence of a uniform transverse magnetic field and asymmetric convective cooling. The mathematical formulation of the problem is established in Section two. In section three the semi-implicit finite difference technique is implemented in time and space for the solution process. In Section four, both numerical and graphical results are presented and discussed quantitatively with respect to various parameters embedded in the flow system.

2. Mathematical model

Consider the transient flow of an incompressible electrically conducting, variable viscosity, reactive third grade fluid placed between two parallel plates induced by the combined action of applied axial pressure gradient and uniform motion of the upper plate. It is assumed that the flow is subjected to the influence of an externally applied homogeneous magnetic field as shown in Fig. 1. The fluid has small electrical conductivity and the electromagnetic force produced is also very small. The plate surfaces are subjected to unequal convective heat exchange with the ambient. The $\bar{x}$-axis is taken along the center of the channel and the $\bar{y}$-axis is taken normal to it.

Following [13–17], and neglecting the reacting viscous fluid consumption, the governing equations for the momentum and heat balance can be written as;

$$\rho\frac{\partial u}{\partial \bar{t}} = -\frac{\partial \bar{P}}{\partial \bar{x}} + \frac{\partial}{\partial \bar{y}}\left[\bar{\mu}(T)\frac{\partial u}{\partial \bar{y}}\right] + \alpha_1\frac{\partial^3 u}{\partial \bar{y}^2\partial \bar{t}} + 6\beta_3\frac{\partial^2 u}{\partial \bar{y}^2}\left(\frac{\partial u}{\partial \bar{y}}\right)^2 - \sigma B_0^2 u, \tag{1}$$

$$\rho c_p\frac{\partial T}{\partial \bar{t}} = k\frac{\partial^2 T}{\partial \bar{y}^2} + \sigma B_0^2 u^2 + \left(\frac{\partial u}{\partial \bar{y}}\right)^2\left(+\bar{\mu}(T) + 2\beta_3\left(\frac{\partial u}{\partial \bar{y}}\right)^2\right) + QC_0A\left(\frac{KT}{\nu l}\right)^m e^{-\frac{E}{RT}}, \tag{2}$$

with the following initial and boundary conditions:

$$u(\bar{y}, 0) = 0, \qquad T(\bar{y}, 0) = T_0, \tag{3}$$

$$u(0, \bar{t}) = 0, \qquad -k\frac{\partial T}{\partial \bar{y}}(0, \bar{t}) = h_1[T(0, \bar{t}) - T_a], \quad \text{for } \bar{t} > 0, \tag{4}$$

$$u(a, \bar{t}) = U, \qquad -k\frac{\partial T}{\partial \bar{y}}(a, \bar{t}) = h_2[T(a, \bar{t}) - T_a], \quad \text{for } \bar{t} > 0, \tag{5}$$

where the additional chemical kinetics term in the energy balance equation is due to [18] and is also illustrated for reacting non-isothermal viscoelastic fluid flow in [19]. Here u is the fluid axial velocity, T is the temperature, T_a is the ambient temperature, T_0 is the fluid initial temperature, $\bar{P}$ is the modified pressure, $\bar{t}$ is the time, ρ is the density, σ is the fluid electrical conductivity, B_0 the electromagnetic induction, k is the thermal conductivity coefficient, c_p is the specific heat at constant pressure, h_1 & h_2 are heat transfer coefficients, Q is the heat of reaction, A is the rate constant, E is the activation energy, R is the universal gas constant, C_0 is the initial concentration of the reacting species, a is the channel half width, l is Planck's number, K is Boltzmann's constant, ν is the vibration frequency, α_1 and β_3 are the material coefficients, m is a numerical constant such that $m \in \{-2, 0, 0.5\}$. The three values taken by the parameter m represent the numerical

exponent for Sensitized, Arrhenius and Bimolecular kinetics respectively (see [3,4,9]). The temperature dependant viscosity ($\bar{\mu}$) can be expressed as

$$\bar{\mu}(T) = \mu_0 e^{-b(T-T_0)}, \tag{6}$$

where b is a viscosity variation parameter and μ_0 is the initial fluid dynamic viscosity at temperature T_0. We introduce the following dimensionless variables into Eqs. (1)–(6);

$$y = \frac{\bar{y}}{a}, \quad \alpha = \frac{bRT_0^2}{E}, \quad W = \frac{u\rho a}{\mu_0}, \quad \theta = \frac{E(T-T_0)}{RT_0^2}, \quad \theta_a = \frac{E(T_a-T_0)}{RT_0^2},$$
$$\gamma = \frac{\beta_3\mu_0}{\rho^2 a^4}, \quad \delta = \frac{\alpha_1}{\rho a^2}, \quad \mathrm{Bi}_1 = \frac{ah_1}{k}, \quad \mathrm{Bi}_2 = \frac{ah_2}{k}, \quad \mathrm{Pr} = \frac{\mu_0 c_p}{k}, \quad \mathrm{Ha}^2 = \frac{\sigma B_0^2 a^2}{\mu_0}$$
$$x = \frac{\bar{x}}{a}, \quad P = \frac{\bar{P}\rho a^2}{\mu_0^2}, \quad G = -\frac{\partial \bar{P}}{\partial x}, \quad \mu = \frac{\bar{\mu}}{\mu_0}, \quad \varepsilon = \frac{RT_0}{E}, \quad t = \frac{\bar{t}\mu_0}{\rho a^2},$$
$$\lambda = \left(\frac{KT_0}{\nu l}\right)^m \frac{QEAa^2C_0 e^{-\frac{E}{RT}}}{T_0^2 Rk}, \quad \Omega = \left(\frac{\nu l}{KT_0}\right)^m \frac{\mu_0^3 e^{\frac{E}{RT}}}{\rho^2 QAa^4 C_0}, \tag{7}$$

and obtain the following dimensionless governing equations;

$$\frac{\partial W}{\partial t} = G - \mathrm{Ha}^2 W + e^{-\alpha\theta}\frac{\partial^2 W}{\partial y^2} - \alpha e^{-\alpha\theta}\frac{\partial \theta}{\partial y}\frac{\partial W}{\partial y} + \delta\frac{\partial^3 W}{\partial y^2 \partial t} + 6\gamma\frac{\partial^2 W}{\partial y^2}\left(\frac{\partial W}{\partial y}\right)^2, \tag{8}$$

$$\mathrm{Pr}\frac{\partial \theta}{\partial t} = \frac{\partial^2 \theta}{\partial y^2} + \lambda(1+\varepsilon\theta)^m \exp\left(\frac{\theta}{1+\varepsilon\theta}\right) + \Omega\left[\mathrm{Ha}^2 W^2 + \left(\frac{\partial W}{\partial y}\right)^2\left(e^{-\alpha\theta} + 2\gamma\left(\frac{\partial W}{\partial y}\right)^2\right)\right], \tag{9}$$

$$W(y,0) = 0, \quad \theta(y,0) = 0, \tag{10}$$

$$W(0,t) = 0, \quad \frac{\partial \theta}{\partial y}(0,t) = -\mathrm{Bi}_1[\theta(0,t) - \theta_a], \quad \text{for } t > 0, \tag{11}$$

$$W(1,t) = 1, \quad \frac{\partial \theta}{\partial y}(1,t) = -\mathrm{Bi}_2[\theta(1,t) - \theta_a], \quad \text{for } t > 0, \tag{12}$$

where λ, Pr, Bi_i, ε, δ, γ, G, α, Ω, θ_a, Ha represent the Frank Kamenetskii parameter, Prandtl number, Biot numbers, activation energy parameter, material parameter, non-Newtonian parameter, pressure gradient parameter, variable viscosity parameter, viscous heating parameter, the ambient temperature parameter and Hartmann number, respectively. The other dimensionless quantities of interest are the skin friction (C_f) and the wall heat transfer rate (Nu) given as

$$C_f = \frac{dW}{dy}(1,t), \quad Nu = -\frac{d\theta}{dy}(1,t). \tag{13}$$

In the following section, the Eqs. (8)–(13) are solved numerically using a semi-implicit finite difference scheme.

3. Numerical solution

Our numerical algorithm is based on the semi-implicit finite difference scheme given in [20] for the isothermal viscoelastic case. As in [19], we extend the algorithm to the temperature equation and take the implicit terms at the intermediate time level $(N+\xi)$ where $0 \le \xi \le 1$. The algorithm employed in [19] uses $\xi = 1/2$, we will however follow the formulation in [20] and thus take $\xi = 1$ in this article so that we can use larger time steps. In fact being nearly fully implicit, our numerical algorithm presented in this article is conjectured to work for any value of the time step! The discretization of the governing equations is based on a linear Cartesian mesh and uniform grid on which finite-differences are taken. We approximate both the second and first spatial derivatives with second-order central differences. The equations corresponding to the first and last grid points are modified to incorporate the boundary conditions. The semi-implicit scheme for the velocity component reads:

$$\frac{\partial}{\partial t}\left(W - \delta\frac{\partial^2 W}{\partial y^2}\right) = G - \alpha\left(e^{-\alpha\theta}\frac{\partial \theta}{\partial y}\frac{\partial W}{\partial y}\right)^{(N)} - \mathrm{Ha}^2 W^{(N+\xi)} + \left(e^{-\alpha\theta} + 6\gamma\left(\frac{\partial W}{\partial y}\right)^2\right)^{(N)}\frac{\partial^2}{\partial y^2}W^{(N+\xi)}. \tag{14}$$

In Eq. (14), forward difference formulas are used for all time derivatives. In particular, given a quantity #, it is understood that $\partial\#/\partial t = (\#^{(N+1)} - \#^{(N)})/\Delta t$. Also the temperature dependent viscosity and shear rate are calculated from the known solution to facilitate the inclusion of the viscous and non-Newtonian terms into the implicit part. By writing $\dot{\gamma}$ for the shear rate, W_y, the equation for $W^{(N+1)}$ then becomes:

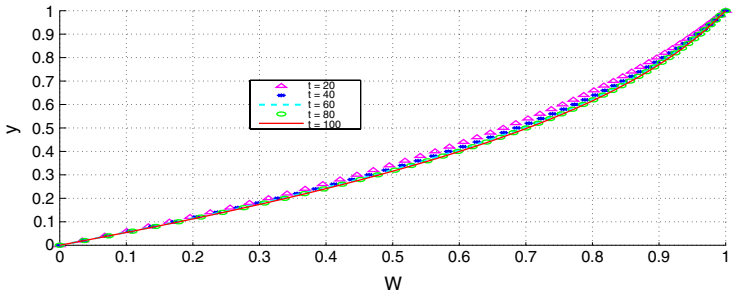

Fig. 2. Transient and steady state velocity profiles.

$$-r_1W_{j-1}^{(N+1)}+(1+2r_1+\Delta t\mathrm{Ha}^2)W_j^{(N+1)}-r_1W_{j+1}^{(N+1)}$$
$$=\Delta tG+(W+\delta W_{yy})^{(N)}-\alpha\Delta t(e^{-\alpha\theta}\theta_y\dot{\gamma})^{(N)}-\Delta t\mathrm{Ha}^2(1-\xi)W^{(N)}+\Delta t(1-\xi)(e^{-\alpha\theta}+6\gamma\dot{\gamma}^2)^{(N)}W_{yy}^{(N)}, \tag{15}$$

where $r_1=[\xi\ \Delta t(\mu+6\gamma\dot{\gamma}^2)^{(N)}+\delta]/(\Delta y^2)$ with $\mu^{(N)}=\exp(-\alpha\theta^{(N)})$. The solution procedure for $W^{(N+1)}$ thus reduces to the inversion of tri-diagonal matrices which is an advantage over a full implicit scheme (i.e. if viscous and non-Newtonian terms are calculated implicitly as well). The semi-implicit integration scheme for the temperature equation is similar to that for the velocity component. Unmixed second partial derivatives of the temperature are treated implicitly:

$$\mathrm{Pr}\frac{\theta^{(N+1)}-\theta^{(N)}}{\Delta t}=\frac{\partial^2}{\partial y^2}\theta^{(N+\xi)}+\lambda\left[(1+\varepsilon\theta)^m\exp\left(\frac{\theta}{1+\varepsilon\theta}\right)\right]^{(N)}$$
$$+\Omega\left[\mathrm{Ha}^2W^2+\left(\frac{\partial W}{\partial y}\right)^2\left(e^{-\alpha\theta}+2\gamma\left(\frac{\partial W}{\partial y}\right)^2\right)\right]^{(N)}. \tag{16}$$

The equation for $\theta^{(N+1)}$ thus becomes:

$$-r\theta_{j-1}^{(N+1)}+(\mathrm{Pr}+2r)\theta_j^{(N+1)}-r\theta_{j+1}^{(N+1)}=\theta^{(N)}+\Delta t(1-\xi)\theta_{yy}^{(N)}+\lambda\Delta t\left[(1+\varepsilon\theta)^m\exp\left(\frac{\theta}{1+\varepsilon\theta}\right)\right]^{(N)}$$
$$+\Omega\Delta t[\mathrm{Ha}^2W^2+\dot{\gamma}^2(e^{-\alpha\theta}+2\gamma\dot{\gamma}^2)]^{(N)}, \tag{17}$$

where $r=\xi\ \Delta t/\Delta y^2$. The solution procedure again reduces to the inversion of tri-diagonal matrices. The schemes (15) and (17) were checked for consistency. For $\xi=1$, these are first-order accurate in time but second order in space. The schemes in [19] have $\xi=1/2$ which improves the accuracy in time to second order. We use $\xi=1$ here so that we are free to choose larger time steps and still converge to the steady solutions. As already conjectured, our algorithm works for any value of the time step! The code was checked for both spatial and temporal convergence. In particular, solutions calculated from, say $\Delta t=1$ using 200 time steps are exactly the same as those after 40 time steps with $\Delta t=5$ or those after 20,000 time steps with $\Delta t=0.01$. Similarly solutions using $\Delta y=0.02$ converge to the same results as those say for $\Delta t=0.025$ or $\Delta t=0.05$ etc. Our code thus runs extremely fast and hence we can easily obtain and thus present all our results at steady state using nearly insignificant computational times.

4. Results and discussion

Unless otherwise stated, we employ the parameter values:
$G=1,\ \mathrm{Pr}=10,\ \theta_a=0.1, \delta=10^{-6}, \lambda=0.1,\ \mathrm{Bi}_1=0.1, \mathrm{Bi}_2=1, m=0.5,\ \varepsilon=0.1, \alpha=0.1, \Omega=0.1, \gamma=0.0001,$ $\Delta y=0.02, \Delta t=1$ and $t=200$.

These will be the default values in this work and hence in any graph where any of these parameters is not explicitly mentioned, it will be understood that such parameters take on the default values.

4.1. Transient and steady flow profiles

We display the transient solutions in Figs. 2 and 3. The figures show a transient increase in both fluid velocity and temperature until a steady state is reached.

4.1.1. Blow up of solutions

We need to point out early on that depending on certain parameter values in the problem, the steady temperature and velocity profiles, such as those shown in Figs. 2 and 3, may not be attainable. In particular, the reaction parameter λ will need to be carefully controlled as "large" values can easily lead to blow up of solutions as illustrated in Fig. 4.

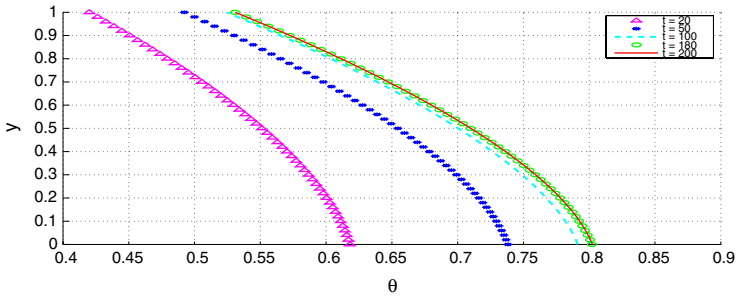

Fig. 3. Transient and steady state temperature profiles.

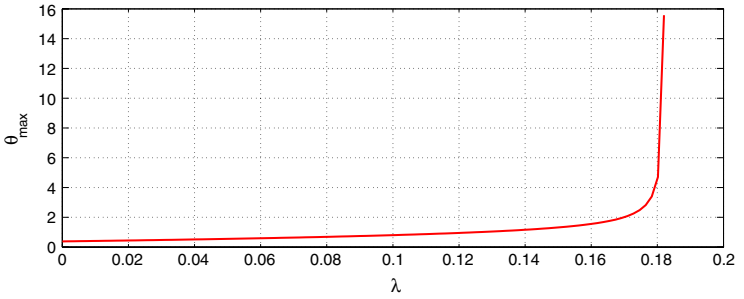

Fig. 4. Blow up of fluid temperature for large λ.

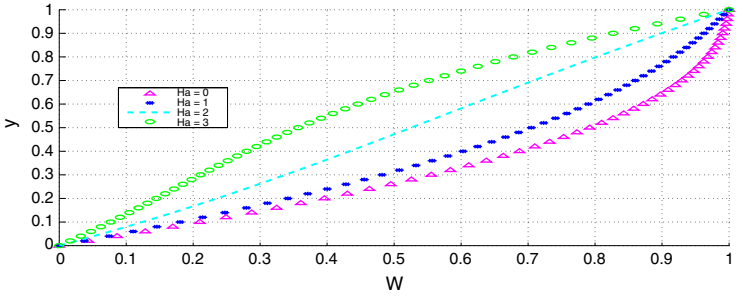

Fig. 5. Effects of Hartmann number (Ha) on velocity.

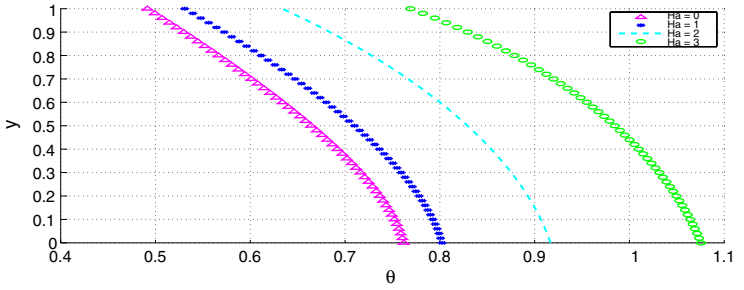

Fig. 6. Effects of Hartmann number (Ha) on temperature.

As shown in Fig. 4, larger values of λ would lead to finite time temperature blow up since the terms associated with λ are strong heat sources.

4.1.2. Parameter dependance of solutions in steady state

It is understood from Figs. 2 and 3 that, at the default parameter, solutions have reached steady state at time $t = 200$. All the steady solutions will thus be understood to be those solutions at $t = 200$.

The response of the velocity and temperature to varying values of the Hartmann number (Ha) is illustrated in Figs. 5 and 6.

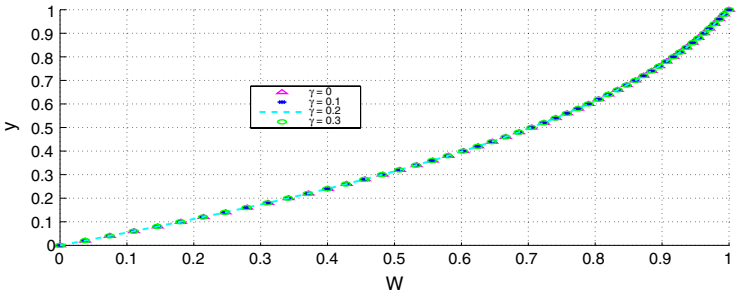

Fig. 7. Effects of non-Newtonian parameter (γ) on velocity.

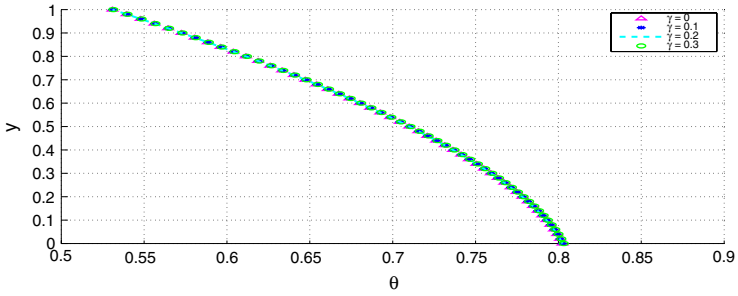

Fig. 8. Effects of non-Newtonian parameter (γ) on temperature.

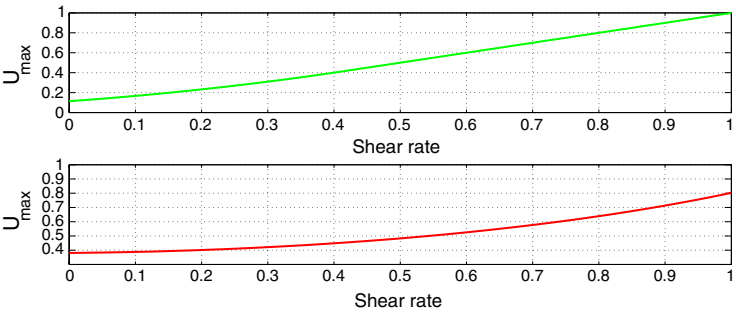

Fig. 9. Effects of shear rate (speed of upper plate).

An increase in the parameter Ha leads to corresponding increases in damping magnetic properties of the fluid. These forces result in increased resistance to flow and thus explain the reduction in fluid velocity with increasing Hartmann number, see Fig. 5. In the temperature equation, the connection of the magnetic field terms to Ω means that the effects of the Hartmann number will closely mirror those of Ω. In particular the Hartmann number appears as a strong source term and hence increases in this parameter correspondingly increases the fluid temperature as shown in Fig. 6.

The response of the velocity and temperature to varying values of the non-Newtonian parameter (γ) is illustrated in Figs. 7 and 8.

Unlike Poiseuille flow, the (Generalized) Couette flow results in very large shear rates. In the latter flow, the shear rate terms hence tend to act as strong source terms in both the energy and momentum equations. As shown in Fig. 9, an increase in the shear rate (speed of upper plate) correspondingly increases both the fluid velocity and temperature.

The parameter γ, which is indeed connected to shear rate terms, hence needs to be kept at low values in the Couette flow case to reduce the strength of these source terms and thus avoid blow up of solutions. At such permissible (low) values of γ both the velocity and temperature profiles hardly show much difference as illustrated in Figs. 7 and 8. It should however be remarked that increasing the value of γ does in fact reduce the velocity, shear rates and hence temperature, see Fig. 10(a).

This is so since γ increases the viscoelasticity of the fluid which in turn reduces fluid velocity and temperature, see for example [19]. However if the values of γ are large, then such reductions in velocity and temperature are insignificant compared to the blow-up effects of the already prevailing shear rates, see Fig. 10(b).

The influence of the variable viscosity parameter on the velocity and temperature profiles is shown in Figs. 11 and 12 respectively.

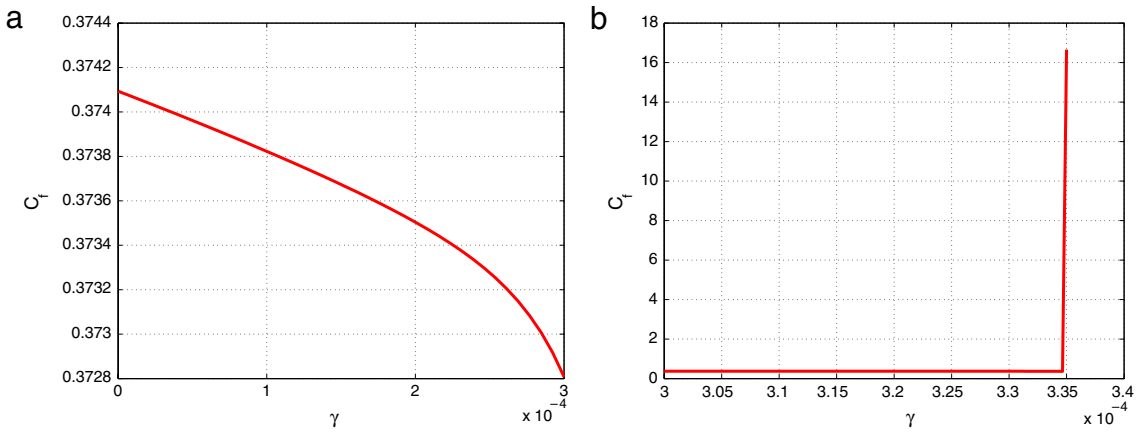

Fig. 10. Effects of γ on shear rate at upper wall (C_f) for Generalized Couette flow.

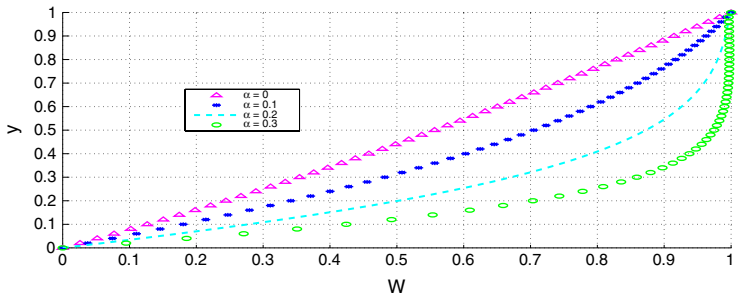

Fig. 11. Effects of variable viscosity parameter (α) on velocity.

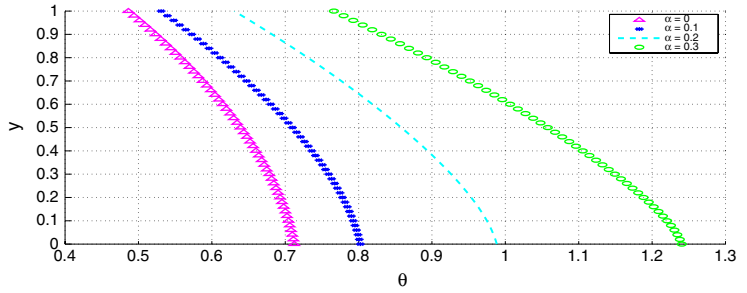

Fig. 12. Effects of variable viscosity parameter (α) on temperature.

Increasing the parameter α reduces the fluid viscosity and hence correspondingly diminishes the fluid's resistance to flow. This necessarily leads to increased fluid velocity as illustrated in Fig. 11. The increased velocity in turn increases the viscous heating source terms in the temperature equation and hence correspondingly increases the fluid temperature as shown in Fig. 12.

The effects of the chemical kinetics exponent m on the velocity and temperature profiles are shown in Figs. 13 and 14 respectively.

Fig. 14 shows that the internal heat generated in the fluid during a Bimolecular type of exothermic chemical reaction ($m = 0.5$) is higher than that generated either under the Arrhenius ($m = 0$) or Sensitized ($m = -2$) reaction types. This is so since an increase in the parameter m leads to corresponding increases in the strengths of the chemical reaction source terms in the temperature equation. This leads to increased fluid temperatures as shown in Fig. 14. Since however the parameter m only enters the velocity equation implicitly through the temperature/viscosity coupling, the effects of m on the fluid velocity at best look marginal and are not as pronounced as on the fluid temperature.

The effects of the activation energy parameter ε on the velocity and temperature profiles is shown in Figs. 15–18. The fluid temperature increases as the ε decreases to zero with maximum temperature at $\varepsilon = 0$, since the case $\varepsilon = 0$ correspond to the extremely volatile nature of the fluid. As with the parameter m, the activation energy parameter only enters the velocity

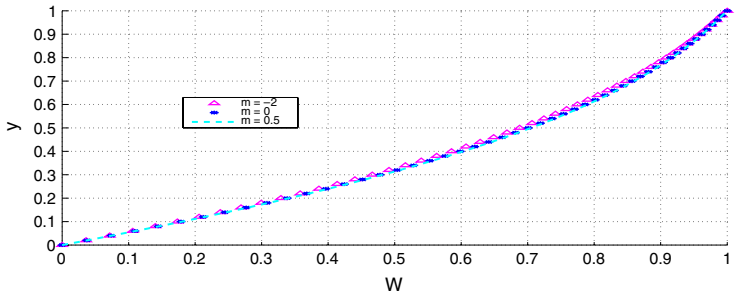

Fig. 13. Effects of parameter (m) on velocity.

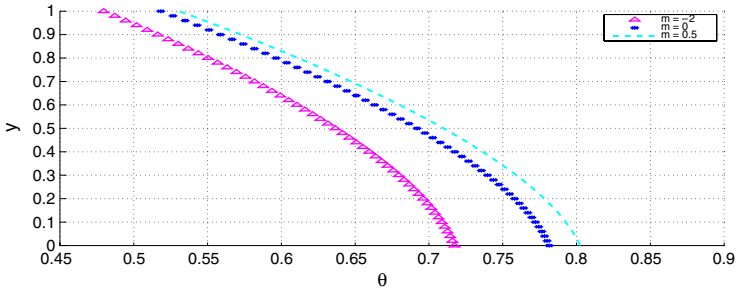

Fig. 14. Effects of parameter (m) on temperature.

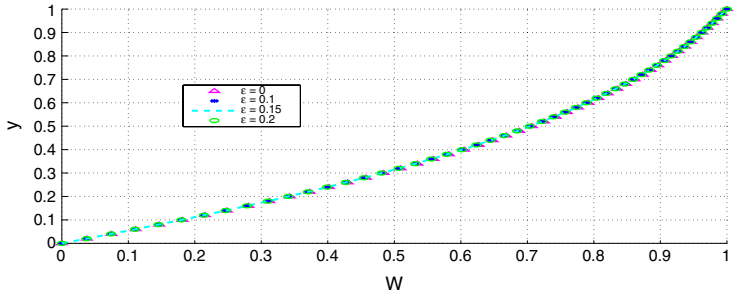

Fig. 15. Effects of activation energy parameter (ε) on velocity.

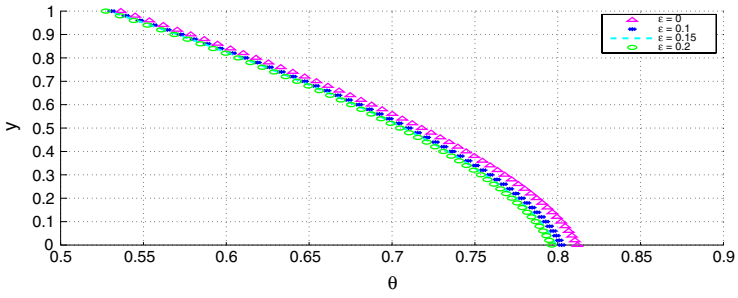

Fig. 16. Effects of activation energy parameter (ε) on temperature.

equation implicitly through the temperature/viscosity coupling. The effects of ε on the fluid velocity thus appear marginal and are not as pronounced as on the fluid temperature.

The effects of the Biot number Bi on the velocity and temperature profiles is illustrated in Figs. 19 and 20 respectively.

As seen from the temperature boundary conditions (11) and (12), higher Biot numbers mean correspondingly higher degrees of convective cooling at the channel walls and hence lead to lower temperatures at the channel walls and hence also in the bulk fluid. The overall temperature profiles thus decrease with increasing Biot number as the bulk fluid continually adjusts to the lower wall temperatures. The reduced temperatures correspondingly decrease the fluid viscosity and hence

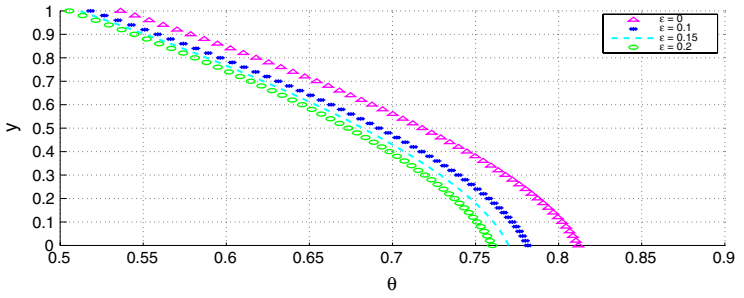

Fig. 17. Effects of activation energy parameter (ε) on temperature, $m = 0$.

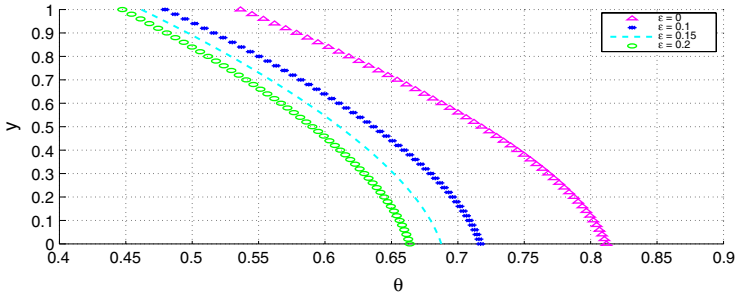

Fig. 18. Effects of activation energy parameter (ε) on temperature, $m = -2$.

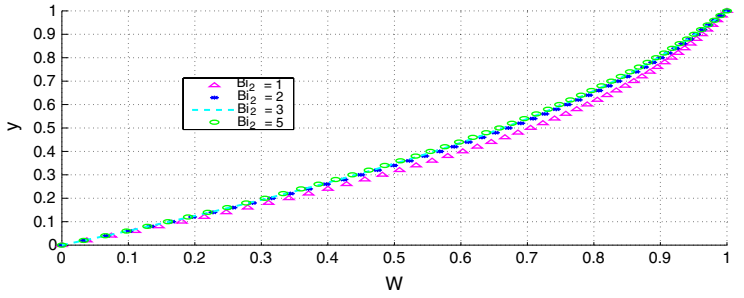

Fig. 19. Effects of the Biot number (Bi) on velocity.

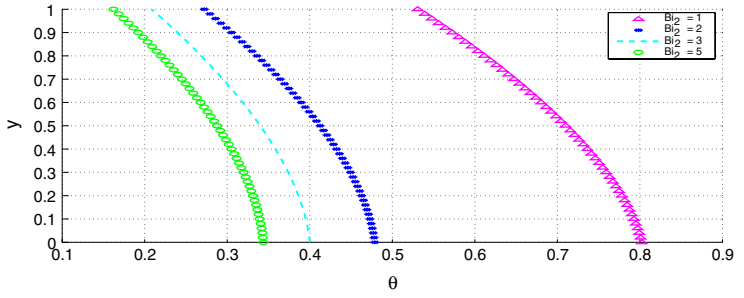

Fig. 20. Effects of the Biot number (Bi) on temperature.

also marginally decrease the fluid velocity through the viscosity coupling. As noted earlier, such a coupling depends on other parameters as well (say α) and hence does not necessarily result in drastic changes in velocity profiles even though the temperature profiles show well pronounced changes, see Figs. 19 and 20.

The effects of the Prandtl number Pr on the velocity and temperature profiles is illustrated in Figs. 21 and 22 respectively.

Larger values of the Prandtl number correspondingly decrease the strength of the source terms in the temperature equation and hence in turn reduce the overall fluid temperature as clearly illustrated in Fig. 22. As pointed out earlier, the reduced temperature results in decreased fluid viscosity and hence reduced fluid velocity, see Fig. 21.

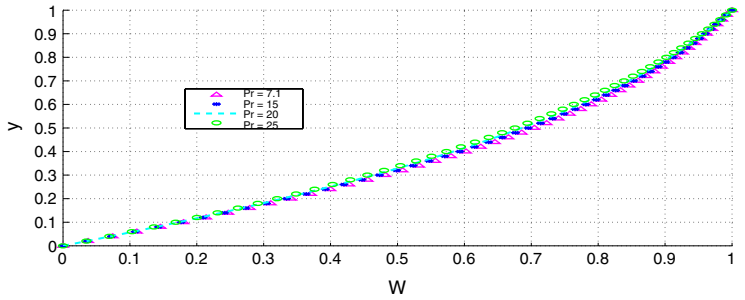

Fig. 21. Effects of the Prandtl number (Pr) on velocity.

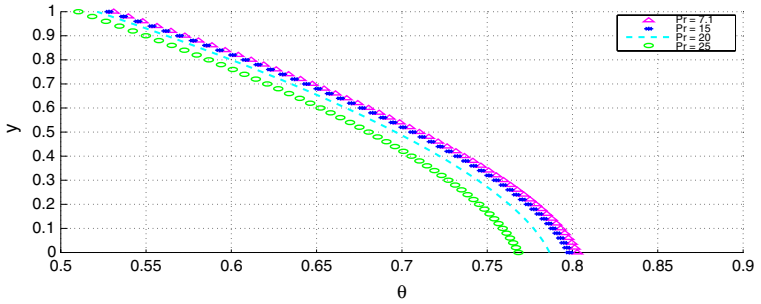

Fig. 22. Effects of the Prandtl number (Pr) on temperature.

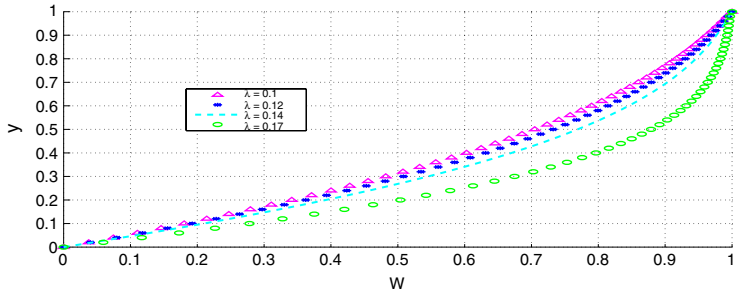

Fig. 23. Effects of the reaction parameter (λ) on velocity.

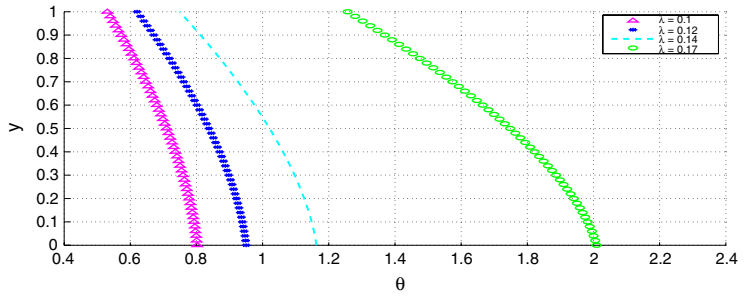

Fig. 24. Effects of the reaction parameter (λ) on temperature.

The effects of the reaction parameter λ on the velocity and temperature profiles is illustrated in Figs. 23 and 24 respectively.

The reaction parameter λ plays a roughly opposite role to the Prandtl number just described. Increased values of λ lead to significant increases in the reaction and viscous heating source terms and hence significantly increase the fluid temperature as shown in 24 and also in the blow up Fig. 4. The significant temperature rise in response to the increased λ mean that the viscosity coupling to the velocity is no longer weak and hence significant reductions in the viscosity (and also the significant increases in temperature gradients) lead to appreciable increases in the fluid velocity.

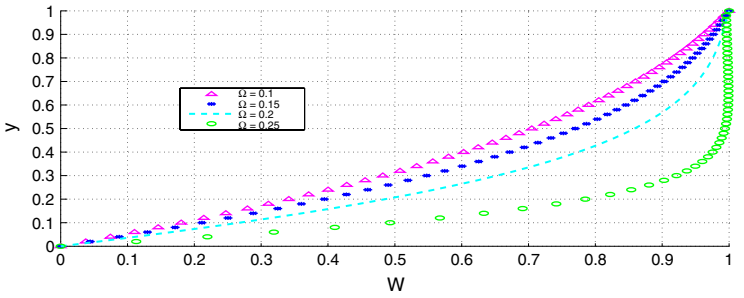

Fig. 25. Effects of the viscous heating parameter (Ω) on velocity.

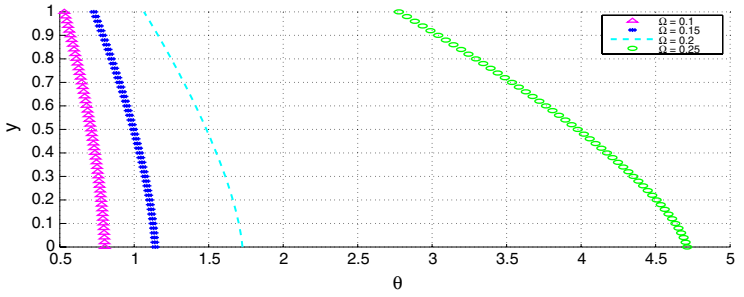

Fig. 26. Effects of the viscous heating parameter (Ω) on temperature.

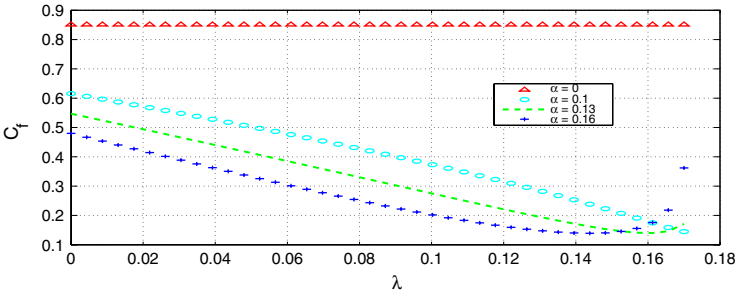

Fig. 27. Variation of wall shear stress with λ and α.

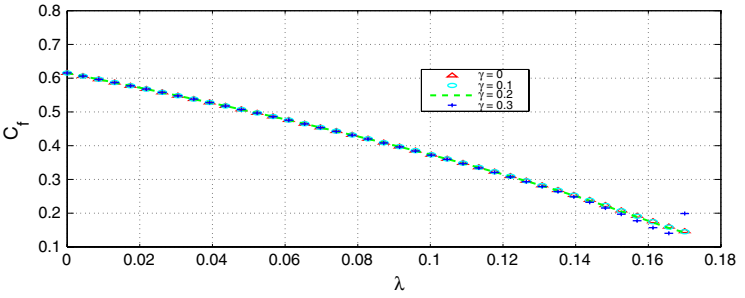

Fig. 28. Variation of wall shear stress with λ and γ.

The effects of the viscous heating parameter Ω on the velocity and temperature profiles is illustrated in Figs. 25 and 26 respectively.

The effects of Ω mirror those of λ, albeit on a smaller scale since Ω is not connected to the exponentially increasing reaction source terms but only to the viscous heating terms.

The wall shear stress dependance on the reaction parameter λ is illustrated in Fig. 27 for varying values of the viscosity variation parameter α. Similarly, Fig. 28 shows the wall shear stress dependance on λ for varying values of the non-Newtonian parameter γ and Fig. 29 shows the wall shear stress dependance on λ for varying values of the Hartmann number

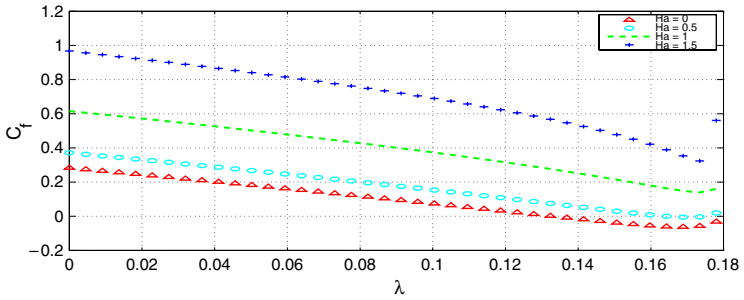

Fig. 29. Variation of wall shear stress with λ and Ha.

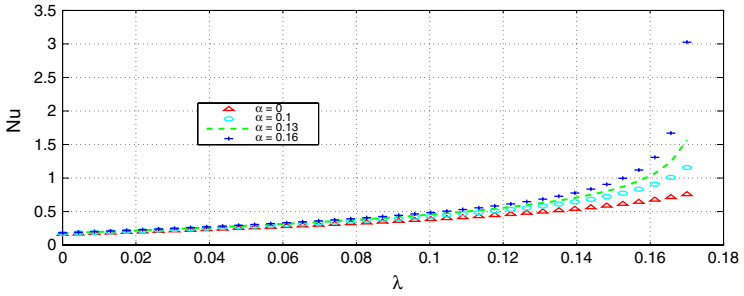

Fig. 30. Variation of wall heat transfer rate with λ and α.

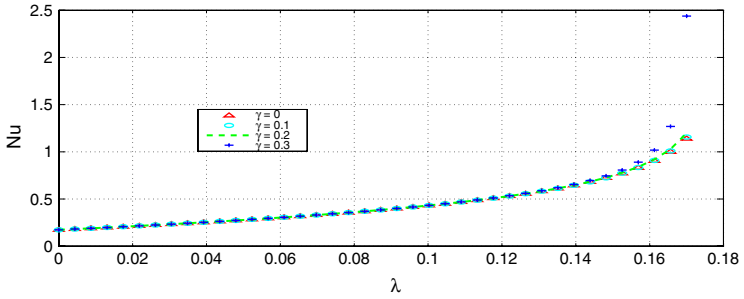

Fig. 31. Variation of wall heat transfer rate with λ and γ.

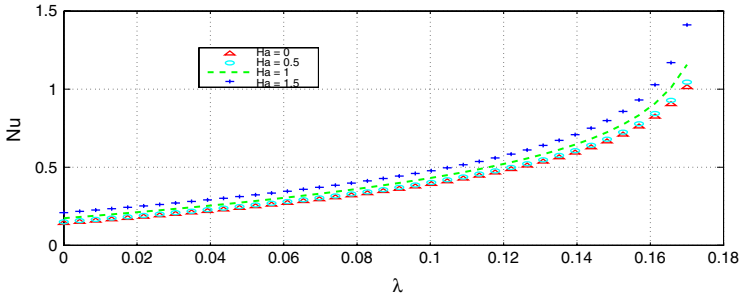

Fig. 32. Variation of wall heat transfer rate with λ and Ha.

Ha. These figures are plotted until the values of λ are reached at which blow-up of solutions sets in. In general, parameters that decrease (increase) the fluid velocity correspondingly increase (decrease) the wall shear stress respectively (increased velocity means decreased slope at upper wall!). Parameters (say λ) that lead to rapid increases in flow quantities need to be carefully controlled, notice the imminent blow up of solutions at the larger α, γ and Ha values even for moderate λ.

The wall heat transfer rate dependance on λ (up to blow-up values) is illustrated in Fig. 30 for varying values of α. Similarly, Fig. 31 shows the wall heat transfer dependance on λ (up to blow-up values) for varying values of γ and Fig. 32 shows the wall heat transfer dependance on λ (up to blow-up values) for varying values of Ha. As with the wall shear stress,

parameters that decrease (increase) the fluid temperature correspondingly decrease (increase) the wall heat transfer. In fact, since both the parameters α and γ only marginally increase the temperature, their effects on the wall heat transfer are also similarly marginal.

5. Conclusion

We develop an unconditionally stable (works for any time step size) and convergent semi-implicit finite difference scheme and utilize it to computationally investigate the transient heat transfer in the hydromagnetic Generalized Couette flow of a reactive third-grade fluid with asymmetric convective cooling. We observe that there is an increase in both fluid velocity and temperature with an increase in the reaction strength, viscous heating and fluid viscosity parameter (which decreases the viscosity). The velocity decreases with the increased magnetic field whereas the temperature is noticed to increase under these conditions. A decrease in both fluid velocity and temperature is observed with an increase in the non-Newtonian character at low values of the non-Newtonian parameter, higher values of this parameter lead to blow up of solutions. The possible finite time blow-up of solutions means also that the reaction strength needs to be carefully controlled.

References

[1] J.A. Shercliff, A Textbook of Magnetohydrodynamics, Pergoman Press, London, 1965.
[2] G.W. Sutton, A. Sherman, Engineering Magnetohydrodynamics, McGraw Hill Book Company, New York, 1965.
[3] K.R. Cramer, S.I. Pai, Magnetofluid Dynamics for Engineers and Applied Physicists, McGraw Hill Book Company, New York, 1973.
[4] J. Hartmann, Theory of laminar flow of an electrically conducting liquid in a homogeneous magnetic field, Hg-Dynamics I, Math. Fys. Med. 15 (1937) 1–28.
[5] J. Hartmann, F. Lazarus, Experimental investigations on the flow of mercury in a homogeneous magnetic field, Hg-Dynamics II, Math. Fys. Med. 15 (1937) 145.
[6] H. Branover, MHD Flow in Ducts, Keter Publ. House Jerusalem Ltd., Wiley and Israel Univ. Press, 1978.
[7] P.A. Davidson, An Introduction of Magnetohydrodynamics, Cambridge Univ. Press, Cambridge, 2001.
[8] C. Truesdell, W. Noll, The non-linear field theories of mechanics, in: Fliigge (Ed.), Handbuch der Physik, vol. 111/3, Springer, Berlin, 1965.
[9] M. Yurusoy, M. Pakdemirli, Approximate analytical solutions for the flow of a third grade fluid in a pipe, Int. J. Non-Linear Mech. 37 (2002) 187.
[10] O.D. Makinde, Thermal criticality for a reactive gravity driven thin film flow of a third grade fluid with adiabatic free surface down an inclined plane, Appl. Math. Mech. 30 (3) (2009) 373–380.
[11] K.R. Rajagopal, On Boundary Conditions for Fluids of the Differential Type: Navier–Stokes Equations and Related Non-Linear Problems, Plenum Press, New York, 1995, p. 273.
[12] R.L. Fosdick, K.R. Rajagopal, Thermodynamics and stability of fluids of third grade, Proc. Roy. Soc. A 339 (1980) 351.
[13] M. Massoudi, I. Christe, Effects of variable viscosity and viscous dissipation on the flow of a third grade fluid in a pipe, Int. J. Non-Linear Mech. 30 (1995) 687.
[14] O.D. Makinde, Thermal stability of a reactive third grade fluid in a cylindrical pipe: an exploitation of Hermite–Padé approximation technique, Appl. Math. Comput. 189 (2007) 690–697.
[15] O.D. Makinde, Hermite-Padé approximation approach to thermal criticality for a reactive third-grade liquid in a channel with isothermal walls, Int. Commun. Heat Mass Transfer 34 (7) (2007) 870–877.
[16] T. Hayat, S. Nadeem, S. Asghar, Hydromagnetic Couette flow of an Oldroyd-B fluid in a rotating system, Int. J. Engng. Sci. 42 (2004) 65–78.
[17] M. Sajid, I. Ahmed, T. Hayat, M. Ayub, Unsteady flow and heat transfer of a second grade fluid over a stretching sheet, Commun. Nonlinear Sci. Numer. Simul. 14 (2009) 96–108.
[18] D.A. Frank Kamenetskii, Diffusion and Heat Transfer in Chemical Kinetics, Plenum Press, New York, 1969.
[19] T. Chinyoka, Computational dynamics of a thermally decomposable viscoelastic lubricant under shear, Trans. ASME, J. Fluids Eng. 130 (12) (2008) 7. 121201.
[20] T. Chinyoka, Y.Y. Renardy, M. Renardy, D.B. Khismatullin, Two-dimensional study of drop deformation under simple shear for Oldroyd-B liquids, J. Non-Newton. Fluid Mech. 31 (2005) 45–56.